Structural Eng./Earthquake Eng. Vol. 9, No. 4, 237s—246s, January 1993
Japan Society of Civil Engineers (Proc. of JSCE No. 459/ I -22)

NUMERICAL SIMULATION OF ULTRASONIC PULSE-ECHO INSPECTION

Chitoshi MIKI*, Kiyohiro IKEDA**,
Kazuo TATEISHI***
and Masanori TAKAHASHI****

This paper presented a numerical simulation of the ultrasonic pulse-echo inspection test, which is potentially a powerful means for QNDE (quantitative non-destructive evaluation) of cracks and flaws of steel structures. The vibration equations of elastic waves for planar rectangular domains with various types of flaws are solved by the finite element method, which can represent flaws of arbitrary shapes. Normal and transverse input ultrasonic pulses are simulated by applying distributed time-varying forces on the boundaries. Wave propagation, reflection, and scattering at the flaws are investigated to draw important information on QNDE. The crack depth is evaluated based on output waves. The validity of the numerical simulation has been shown by the comparison between analysis and experiment.

Keywords : *cracks, elastic waves, QNDE, scattering, ultrasonic pulse-echo inspection*

1. INTRODUCTION

Ultrasonic pulse-echo inspection test locates and sizes of flaws (cracks and voids) in structural members based on the intensity and the transit time of reflected ultrasonic waves. This method, which has already been employed in many engineering fields, is emerging as the most promising QNDE (quantitative non-destructive evaluation) method for structures. The application of this method will be further extended, while its major drawbacks, such as the lack of recordability and objectivity, are rapidly being addressed through the progress in automatic measurement and in multi-scope visualization of ultrasonics[1),2)].

Fracture mechanics and relevant experimental procedures have been developed as to be capable of accurately estimating fracture and fatigue life. However, inaccuracy of data for fracture mechanics, such as the location, the shape and the size of flaw and defect estimated by the pulse-echo inspection, is currently degrading the overall accuracy. In order to develop a more accurate and dependable QNDE technique, we investigate in this paper basic properties of an ultrasonic pulse echo by solving vibration equations of elastic waves, and draw quantitative information on flaws based on reflected and diffracted waves.

Various kinds of analytical solutions[3~8)] of elastic waves have been derived for the scattering of an ultrasonic echo at flaws. For example, Sih and Loeber[3)] obtained the solution of reflection and diffraction at a crack when a sinusoidal wave is input with an incident angle.

These equations have also been solved by typical numerical techniques, including finite difference[9)], finite element[10)], and boundary element methods[11)~13)]. Further the Ootsuki model, which combines the particle model and the finite element method, was put to use in the computer simulation of ultrasonics[14)~16)]. An inverse problem[17)] has been presented as a means to determine the shape of a crack. These analytical and numerical techniques and their visualization provide us with information on scattered waves at the flaws.

This paper presents a numerical simulation of the propagation and reflection of an ultrasonic pulse echo in a steel plate by means of finite element analysis, which is capable of representing flaws of arbitrary shape and is suited for visualization of simulation results. Based on this numerical simulation, suggestions on the ultrasonic pulse-echo method are presented to make it more accurate and quantitative. The validity of the simulation is assessed based on the comparison between analysis and experiment.

2. EXPERIMENT

Ultrasonic pulse-echo inspection test was performed on a parallelepiped steel plate shown in **Fig.1.**

Normal and angled probes with the properties listed in **Table 1** were employed. Recall that the analysis employed different frequency for the input probe than experiment so as to reduce the computational cost. As shown in **Fig.2,** three probes 1, 2,

* Member of JSCE, Dr. Eng., Professor, Dept. of Civil Eng., Tokyo Inst. of Tech. (Meguro-ku, Tokyp 152, Japan)
** Member of JSCE, Ph.D., Assoc. Prof., Dept. of Civil Eng., Nagaoka Univ. Tech.
*** Member of JSCE, M. Eng., Research Assoc., Dept. of Civil Eng., Tokyo Inst. of Tech.
**** Member of JSCE, Graduate Student, Dept. of Civil Eng., Tokyo Inst. of Tech.

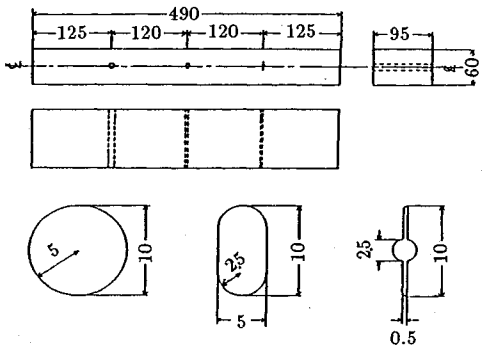

Fig.1 Steel test specimen

Table 1 Properties of ultrasonic probes.

	Type
Normal	V109 5MHz 0.5inϕ
Angled	5MHz 10×10 A45 (standard)
	5MHz 1/4inϕ (high resolution)

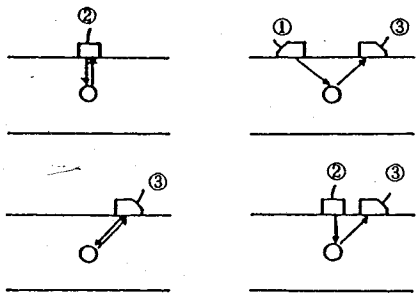

Fig.2 Location of Probes.

and 3 were allocated in such a manner that incidental waves were directed toward the top of those flaws. Probes 1 and 3 are 45-degree angled ones, and probe 2 is a normal one. It is customary to input and measure the echo by the same probe. For example, probe 2 is used to input and measure normal waves for the normal wave method, and for the angled one probe 1 (or 3) is used to do transverse ones. In this paper other output probes, however, are also used to measure output waves to acquire more information on flaws. **Fig.3** shows typical pulses measured in this manner.

Fig.4 shows an ultrasonic pulse which was input with a 45-degree-angled probe on the surface and measured with another probe on the bottom surface. The ordinate denotes the voltage of the pulse measured, and the abscissa expresses the time. Although this measured pulse may involve some experimental errors, it presumably is quite similar to a typical input pulse, which is to be accurately simulated in analysis.

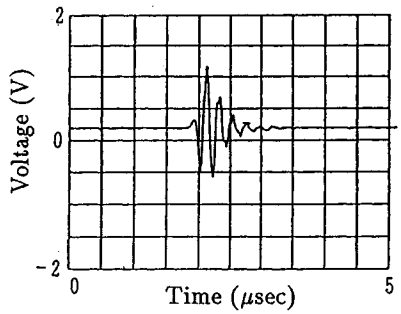

(a) Circular hole

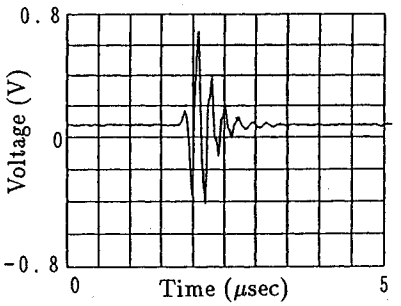

(b) Slot hole

Fig.3 Measured pulse echo for the normal wave method (input at probe 2, and measured at probe 1).

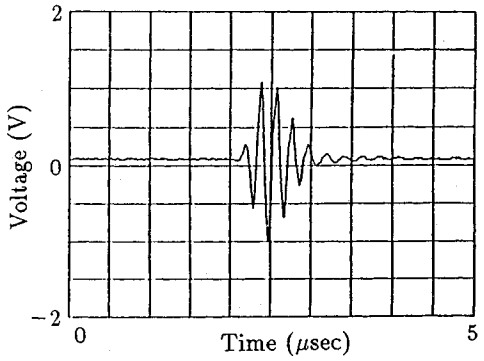

Fig.4 Measured ultrasonic pulse.

3. NUMERICAL SIMULATION

(1) Numerical modeling

We performed numerical simulation of ultrasonic pulse-echo test for the test specimen shown in **Fig.1** with three typical flaws, including : (a) a circular hole, (b) a slot hole, and (c) an infinitesimally thin slit. The radius of tip of these three flaws is 2 mm, 1 mm, and 0 mm, respectively.

Three 14×28 mm elastic rectangular domains with these flaws, shown in **Fig.5**, were employed as numerical models of this specimen: A pair of slit surfaces are assumed to be free boundaries which do not exert contact forces. The upper surface of

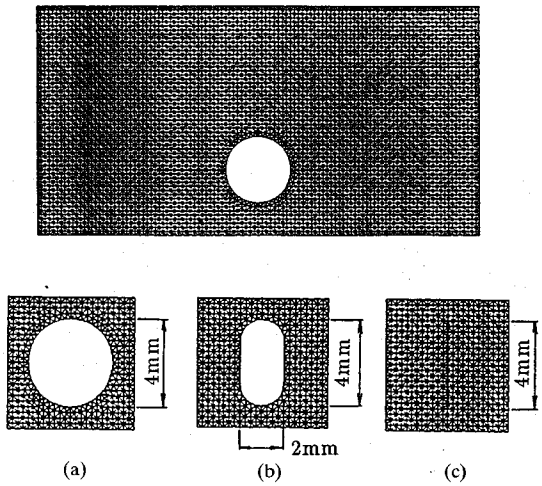

Fig.5 Rectangular domain with three types of flaws.

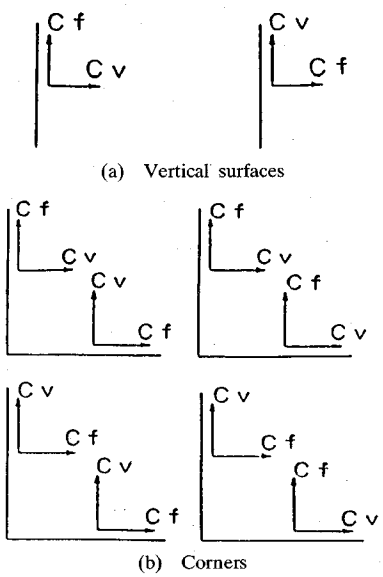

Fig.6 No reflection boundaries.

these domains is free boundary. The right, the left, and the bottom surfaces, where the domains were cut out from the steel plate, are no-reflection boundaries of Cundall's method[18], which annihilate reflection waves by superposing two reflection waves with a phase lag of π radians. We here employed reflection waves corresponding to two boundary conditions : uniform constant external force C_v and uniform constant velocity C_f as shown in **Fig.6** (a) ; these constants were chosen in such a manner that numerical results are most stabilized. Reflection waves, however, cannot be removed in this manner at the corners of two no-reflection boundaries, where an incidental waves is reflected twice at different boundaries. Instead of this, a

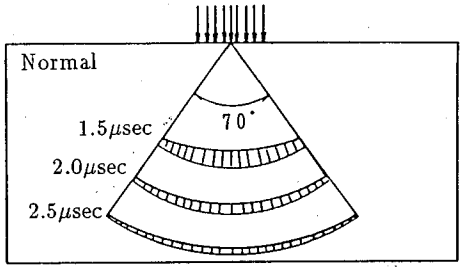

Fig.7 Simulation of normal wave.

revised one in **Fig.6** (b) with four different boundary conditions were employed. It was suffice to perform the superposition only for a few time steps and, as well as, for a few meshes in the vicinity of boundaries.

The vibration equations discretized by the finite element method are expressed as :

$$M\ddot{v}+Kv=P(t), \quad \cdots\cdots(1)$$

where M is a concentrated mass matrix ; v is a displacement vector ; ($\dot{}$) denotes the differentiation with respect to the time t ; K is a stiffness matrix defined by means of a triangular one-dimensional element ; $P(t)$ is an external force vector.

We employed input ultrasonic waves with the frequency of 2 MHz. The wave speed for a longitudinal (compressional) wave is 5900 m/s and that for transverse (shear) one is 3200 m/s. The wave length of a longitudinal wave, accordingly, is 3.0 mm, and that for transverse one is 1.6 mm. The mesh size of finite elements shown in **Fig.5** was chosen to be 0.25 mm*, which is approximately equal to 1/10 of the wave length for the longitudinal wave and to 1/6 of that for the transverse one.

Newmark's β method with $\beta=1/6$ was used to obtain $v(t)$ by numerically integrating Eq. (1). A time resolution of 0.025 μs, which corresponds to 1/20 of the period of the input ultrasonic pulse, was employed.

(2) Input pulses

In the present analysis, input pulses by normal and angled probes were simulated by applying time varying forces of a period of sine wave over the length of 4 mm of the top surface of the specimen. For a normal probe, vertical external forces with varying amplitudes were applied without a time lag. The propagation of wave initiated by these forces can be seen in **Fig.7,** which shows the vector view of displacement at the time of $t=1.5$, 2.0, and

*We performed a series of preliminary analysis with finer meshes, such as 0.15 mm, to insure the adequacy of the mesh size so as to accurately simulate the vector views in **Fig.10** and the time histories in **Fig.12**.

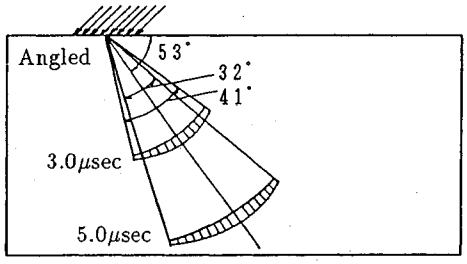

Fig.8 Simulation of transverse wave.

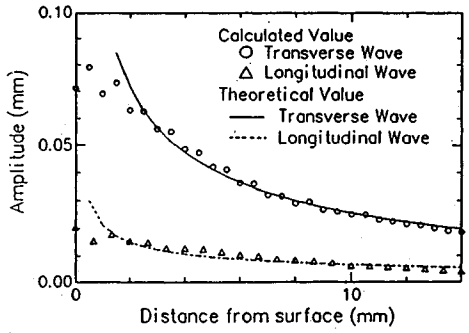

Fig.9 Damping properties of simulated waves.

2.5 μs. Here the length and the direction of a line denote the magnitude and the direction of displacement at the relevant point. The angles in this figure denote the range where the magnitude of displacement exceeds 50 percent of the relevant maximum displacement. An input pulse for a normal probe, which propagates primarily to a vertical direction, has thus been well simulated.

The input transverse wave of an angled probe was simulated by applying a series of forces with an incident angle of 45 degrees, as shown in **Fig.8.** These forces were applied with time lags so as to accurately simulate the shape of wave front. Most of input waves then were transformed into transverse ones due to the critical angle. As can be seen, a transversal wave traveling in a 45-degree-angled direction is well represented.

The damping properties of these waves are plotted in **Fig.9.** The ordinate denotes the amplitude and the abscissa the distance from the probe. The solid lines denote the theoretical curve of the damping of planar elastic waves. The amplitudes of longitudinal and transverse waves damp with the $-1/2$ power of the distance, in agreement with the theory of planar elastic waves.

(3) Wave propagation

Vector views of propagation, reflection, and diffraction of ultrasonic waves are shown in **Fig.10** for various cases, including : (a) the normal wave method for the circular hole, (b) the same method for the infinitesimally thin slit, (c) the angled wave

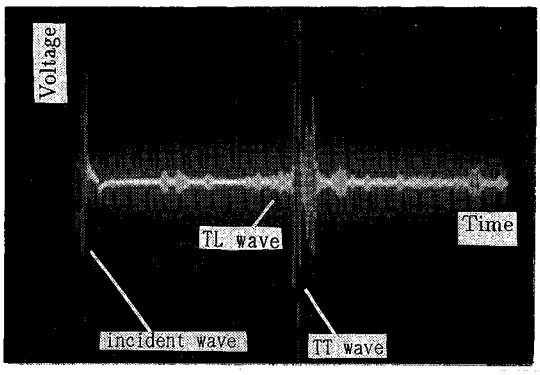

Photo 1 Measured ultrasonic pulse (angled wave method ; circular hole).

method for the circular hole, (d) that for the slot hole, and (e) for the slit. Longitudinal waves, with a higher speed, form the outer front of incidental waves, whereas slower transverse ones their inner front. Both of these incidental waves are reflected and diffracted at the flaws into longitudinal and transverse waves. Reflected longitudinal and transverse waves of an incident longitudinal wave are usually called LL and LT waves, respectively ; those of an incident transverse wave are TL and TT ones, respectively. In addition, tip echo (cylindrical wave) exists for a slit. It is vital in the success in an ultrasonic pulse-echo inspection to identify these five types of waves separately. The time history of a pulse echo measured for a circular hole with an incidental transverse wave is shown in **Photo 1,** which clearly displays the peaks of TL and TT ones.

For the normal wave method, transverse waves are absent at probe 2, and as well as, on the center line connecting probe 2 and the top of a flaw, as shown in **Fig.10** (a) and (b). Such absence of transverse waves, which arises from the reflection symmetry about the center line, makes this probe plausible in the ultrasonic inspection. Strong reflection waves exist at both the circular and the slot holes, irrespective of the direction of input waves. By contrast, almost all waves pass by the infinitesimally thin slit for the normal wave method, and hence there exist very weak reflection waves. For the thin slit for the angled method relatively strong cylindrical waves, which are to be employed in the tip echo method, are diffracted from the sharp edge of the slit. The tip echo from the top edge, which has been observed in 16) , cannot be clearly seen in the present analysis.

Very strong direct surface Rayleigh waves are propagating on the top surface for each case. In the experiment, such surface waves, which are removed by mode transformation and by attaching an

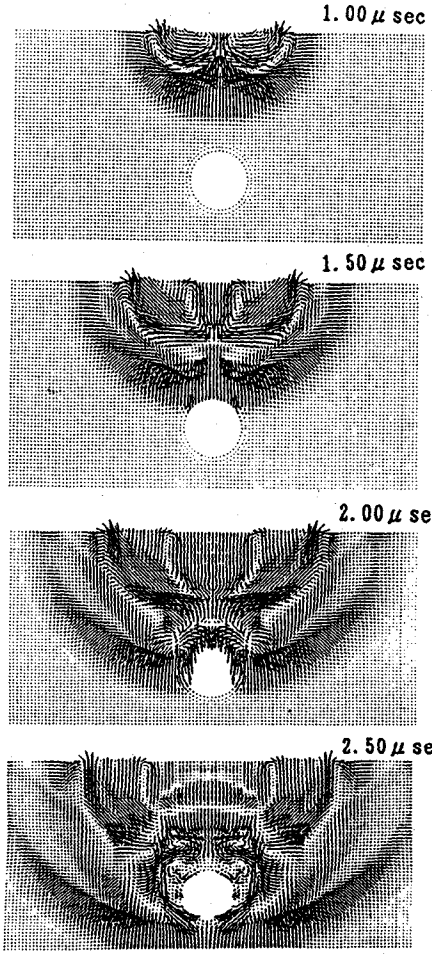

(a) Normal wave method ; circular hole

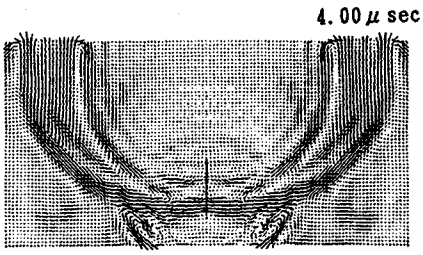

(b) Normal wave method ; slit

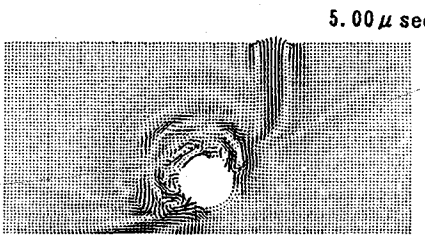

(c) Angled wave method ; circular hole

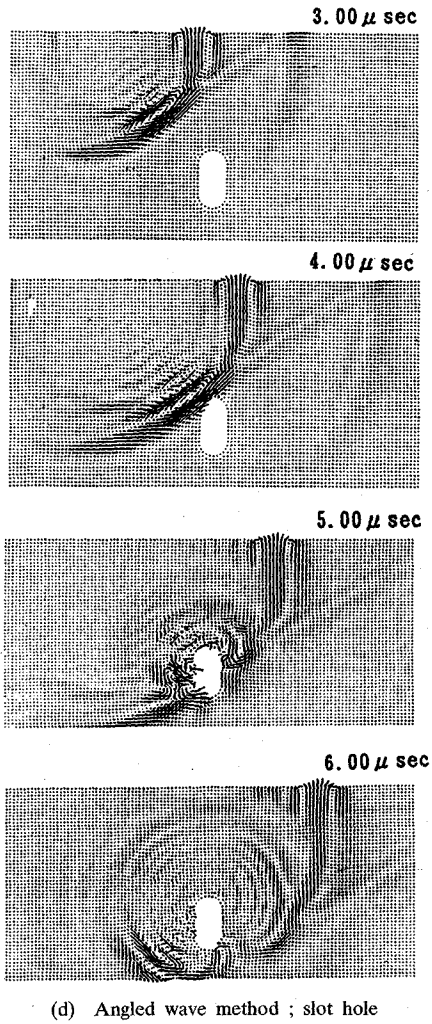

(d) Angled wave method ; slot hole

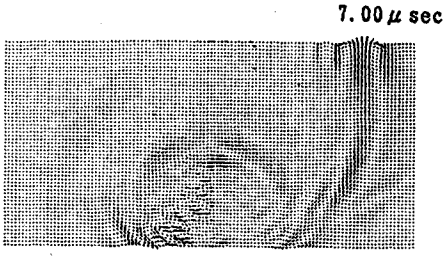

(e) Angled wave method ; slit

Fig.10 Vector views of propagation and reflection of ultrasonic waves.

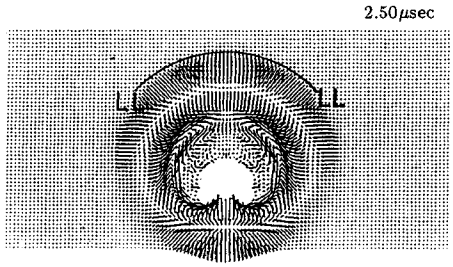

(a) Normal wave method ; circular hole

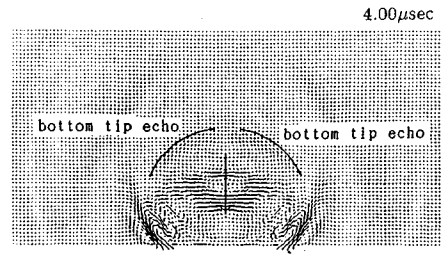

(b) Normal wave method ; slit

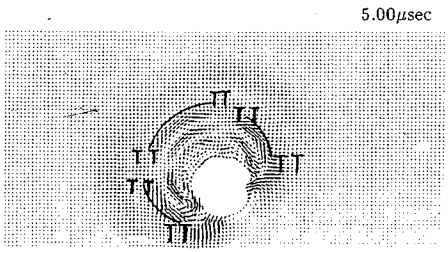

(c) Angled wave method ; circular hole

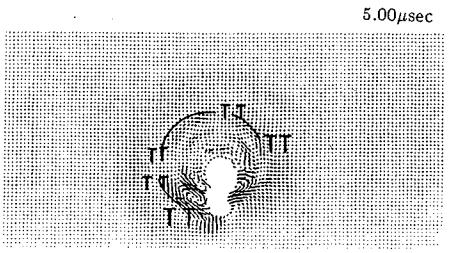

(d) Angled wave method ; slot hole

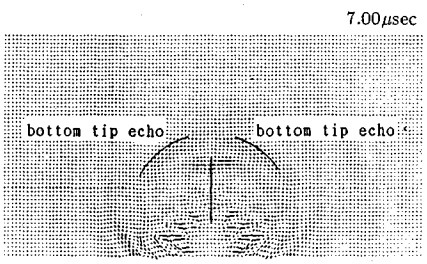

(e) Angled wave method ; slit

Fig.11 Vector views of $v^*(t)$.

absorbant on the surface of the specimen, are not predominant. To be consistent with this experimental environment, we removed surface waves by performing a subtraction

$$v^*(t)=v(t)-\hat{v}(t) \quad \cdots\cdots(2)$$

where $v^*(t)$ indicates the displacement vector for a scattered wave ; $v(t)$ denotes that with a flaw ; $\hat{v}(t)$ expresses that without it.

Fig.11 shows vector views of $v^*(t)$ for various cases. Reflection waves at flaws and diffracted ones at the tip can be seen much clearer, compared with the vector views of $v(t)$ in **Fig.10.** In particular, the presence of bottom tip echo can be seen for a slit in (b) and (e) .

Fig.12 shows an example of this subtraction for the wave input at normal probe 2, reflected at the circular hole, and measured at the same probe. The time histories of $v(t)$ and $\hat{v}(t)$, with and without the hole, are greatly influenced by the surface waves, so that a scattered wave cannot be identified with ease. The subtracted displacement $v^*(t)$, by contrast, clearly shows the presence of a scattered wave, and hence will be used in the remainder of this paper.

4. APPLICATION TO QNDE

(1) Normal wave method

For a normal wave pulse input and measured at probe 2, time histories of $v^*(t)$ shown in **Fig.13** were computed for the aforementioned three types of flaws. All of these waves consist of longitudinal waves, as we have already seen in **Fig.10** (a) and (b). From the speed of the longitudinal and transverse waves, one can compute that scattered LL wave arrives at probe 2 at $t=2.7$ μs and TL wave at $t=3.9$ μs. Hence the first (two) peaks correspond to a pure LL wave, which will present more accurate information on the flaws ; and the other peaks to the combination of LL and TL waves, which yield less accurate one.

Fig.14 shows time histories of $v^*(t)$ input at probe 2 and measured at probe 1, at which both longitudinal and transverse waves arrive. In order

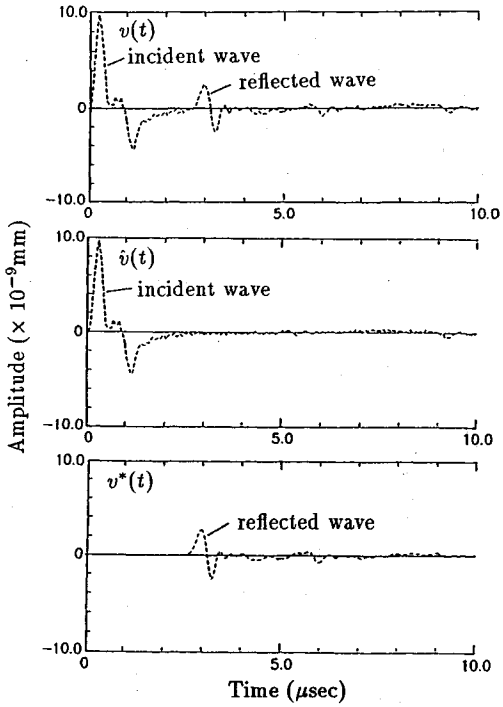

Fig.12 Removal of surface wave (normal wave method; input and measured at probe 2).

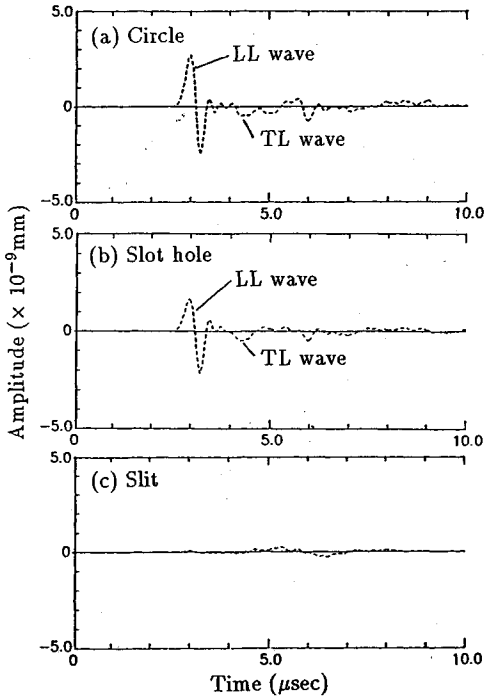

Fig.13 Displacement history of $v^*(t)$ for the normal wave method (input and measured at probe 2).

to identify these two types of waves, reflected waves were assumed to propagate toward the direction between probe 1 and the top of a flaw. Then the waves were decomposed into two components : a wave toward this direction (denoted by dashed lines in the figure) and its orthogonal component (by solid lines). The former is expected to be close to the longitudinal wave, and the latter to the transverse one.

Scattered LL, and TT waves arrive at probe 1 at $t = 3.3$, and 6.0 μs, respectively. The first (two) peaks in **Fig.14** which consist of pure LL wave, are suggested for use in drawing information on the flaws. For a slit, a weak response can be seen approximately at $t = 7.0\ \mu s$. This probably is the tip echo reflected from bottom edge of the slit, based on the delayed arrival time and also on the relevant vector view in **Fig.11.**

In the current ultrasonic pulse-echo test system,we can measure only the magnitude of the total wave, which is the sum of longitudinal and transverse components. In consistent with this experimental situation, we estimated the depth of the three types of flaws based on the first peak of the total wave. This peak, which consists mostly of LL waves, are expected to present accurate information on the flaws. The depth of the flaws for this case is expressed as :

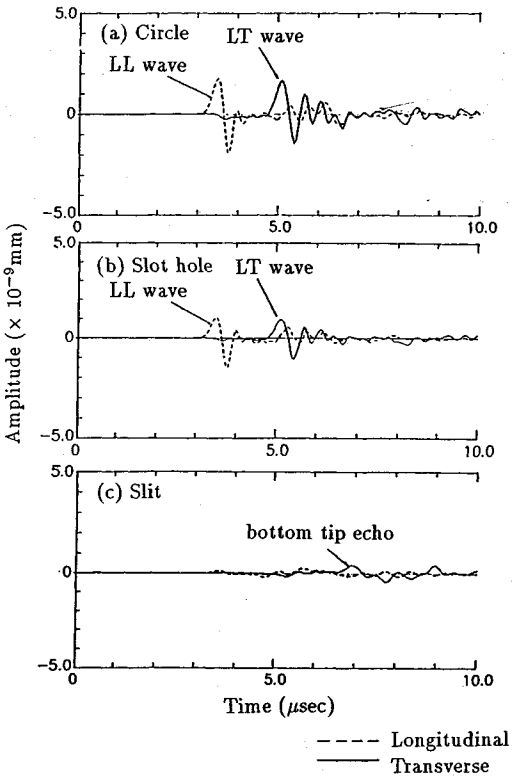

Fig.14 Displacement history of $v^*(t)$ for the normal wave method (input at probe 2 and measured at probe 1).

Table 2 Estimated depth of the flaws for input probe 2.

Type of flaws	Measuring probe	
	1	2
Circular hole	7.82	7.89
Slot hole	8.13	7.82
Thin slit	8.13	8.11

(Unit in mm; exact value is 8.00 mm).

Table 3 Estimated depth of the flaws for input probe 1.

Type of flaws	Measuring probe	
	1	2
Circular hole	8.06	8.02
Slot hole	8.06	8.06
Thin slit	8.20	8.12

(Unit in mm; exact value is 8.00 mm).

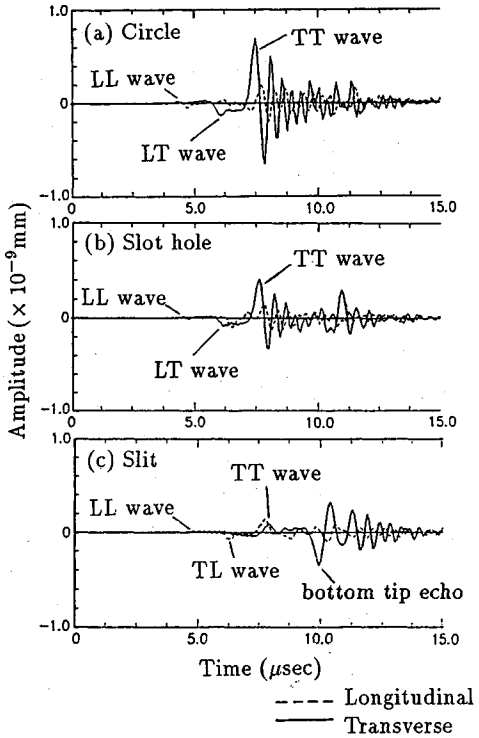

(a) Measured at probe 1

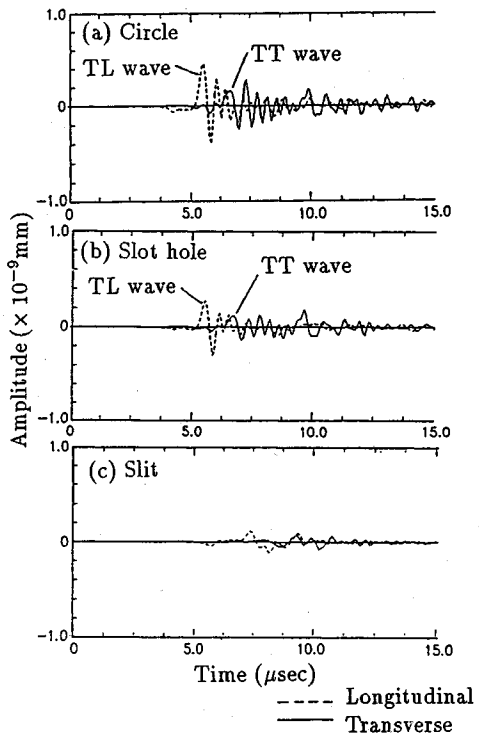

(b) Measured at probe 2

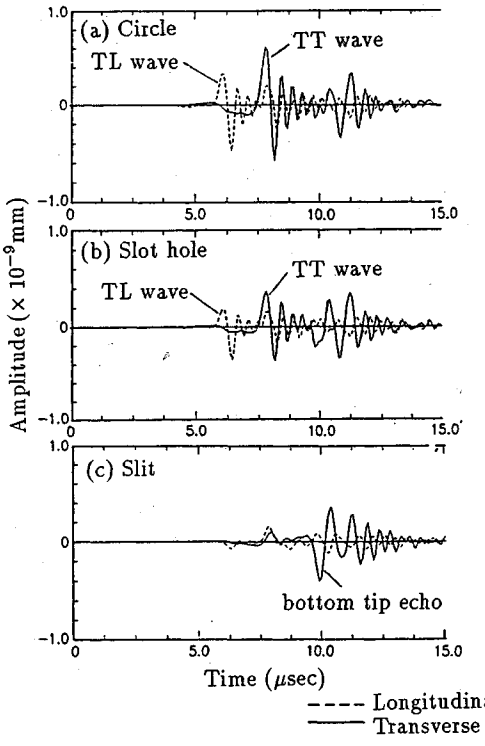

(c) Measured at probe 3

Fig.15 Displacement history of $v^*(t)$ for the angled wave method (input at probe 1).

$$(t_p - t_0) \times \frac{c}{r} \quad \cdots\cdots (3)$$

where c is equal to the wave speed for a longitudinal wave (5900 m/s) ; t_p is the arrival time of the first peak of the total wave ; $t_0=0.25\ \mu s$ denotes its starting time ; and

$$r=\begin{cases} 1+\sqrt{2} & \text{probe1,} \\ 2 & \text{probe2.} \end{cases}$$

The values of the depth estimated by Eq. (3) for output probes 1 and 2 are listed in **Table 2.** These values correlate well with the exact value of 8.0 mm, thereby showing the validity and usefulness of the present simulation and, as well as, the ultrasonic inspection. Note that the arrival time is not necessarily the same as the exact value because the displacement time history is obtained as a superposition of a series of waves reflected at different points on the flaws, and its peak is inevitably obscured.

For both output probes, the circular hole, the slot hole, and the thin slit displayed stronger scattered waves in this order. The first few peaks of the displacement time histories for the circular and the slot holes are sufficiently clear as to serve as quantitative information. Such a tendency has also been observed in the relevant experiment.

Care must be taken in drawing information on the thin slit, the response of which consists mainly of very weak and obscure tip echo (cylindrical waves). Probe 1, which has greater response, may be more advantageous as a measuring probe.

(2) Angled wave method

For an angled transverse wave input at probe 1, we computed the displacement histories shown in **Fig.15** measured at each of the three probes for the three types of flaws. Scattered LL, TL, LT, and TT waves reach probe 1 approximately at $t=3.8$, 5.4, 5.4, and 7.0 μs, respectively ; the tip echo reaches it after these waves.

For probe 1 (**Fig.15** (a)) TT wave for the circular or slot hole is quite strong and discernible, while LL, and LT waves are weak and indiscernible. The response for a slit with small amplitudes was quite obscure. After $t=10\ \mu s$, strong peaks can be seen for each of the three types of flaws.

For probe 2, TT wave, which arrives at $t=6\ \mu s$, has the same or less magnitude than other type of waves. Further, this wave is significantly influenced by LT wave. TT wave, accordingly, cannot be accurately acquired in the experiment due to the presence of a strong longitudinal wave after $t=6\ \mu s$. Further the tip echo cannot be observed clearly. This probe, accordingly, is not good for measuring point.

For probe 3 relatively strong TL wave is observed in addition to TT waves. The tip echo can be observed clearly.

To sum up the angled wave method with greater tip echo is good for measuring it ; probes 1 and 3 are good measuring points for TT wave. We estimated the depth of flaws by Eq. (3) for TT wave and listed it in **Table 3** for probes 1 and 3. Here we used $c=3200$ m/s, $t_0=0.6\ \mu s$, and

$$r=\begin{cases} 2\{[1+(a/8)^2]^{1/2}-a/8\} & \text{probe1,} \\ 2\sqrt{2} & \text{probe3,} \end{cases}$$

where a is the radius of a flaw. Again the estimated depth is fairly accurate.

5. REMARKS ON TIP ECHO

Strong tip echo has been observed both for normal and angled wave methods for all three types of flaws in **Fig.15.** The following hypothesis is proposed here as a mechanism to produce such echo : (1) the incidental wave is transformed into a surface wave at the onset of reaching the surface of a flaw ; (2) this surface wave propagates on the surface of the flaw from top to bottom ; and (3) for a slit this wave becomes a tip echo upon reaching its bottom ; for the circular and the slot holes it comes back from bottom to top and then bounces back into the steel plate. The first peak of the tip echo for the slit seems to have a positive deflection, while that for the circular or slot holes have negative one. Its wave form is somewhat obscure and more studies are required in the future. This mechanism is in good agreement with the well known hypothesis that the top and the bottom echoes have a time lag of half wave length. Similar description can be found in the handbook[19] for the tip echo method.

Since the travelling distance on the surface wave is shorter for the slit, the slot ,and the circular holes in thin sequence, the magnitude of the tip echo should be greater and their arrival time is earlier in this sequence. Such features are in good agreement with the numerical results in **Fig.15.** It will be a topic to be studied further to acquire quantitative information from the tip echo.

6. CONCLUDING REMARKS

Mixed presence of various types of waves obscures the peak of pulse echo, thus degrading the accuracy of QNDE of crack depth. As an attempt to systematically identify such waves, surface Rayleigh waves have been removed, and longitudinal and transverse waves have been separated.

ACKNOWLEDGEMENT

The writers are grateful to Masahiko Kato of the Bridge Inspection Center and to Shouichi Umeda

of Horosotec for performing ultrasonic inspection test and for offering important suggestions. The assistance of Mr. Masahiro Yoshimi and Mr. Tomoo Okinaka for the development of computer program especially at the earlier stage, is greatly appreciated. This study is supported in part by the Grant-in Aid for General Scientific Research from the Japanese Ministry of Education, Science and Culture (NO.03452200).

REFERENCES

1) Miki, C., Fukazawa, M., Katoh, M., and Ohune, H. : Feasibility study on crack detection of fillet welded joint, Proc. of JSCE, No. 386, pp. 329-337,1987 (in Japanese).
2) Iijima, T., Hukami, M., Miki, C., and Tajima, J. : Study on fatigue crack detection in stiffening truss chord members, Proc. of JSCE,No. 410, I-12, pp. 445-454, 1989 (in Japanese).
3) Loeber, J. F., and Sih, G. C. : Diffraction of antiplane shear waves by a finite crack, Acoust. Soc. Amer. 44, pp. 90-98, 1968.
4) Mal, A. K. : Interaction of elastic waves with a Griffith Crack, Int. J. Engng Sci., Vol. 8, pp. 763-776, 1970.
5) Ryan R. L., and Mal, S. : Scattering of antiplane shear waves by a submerged crack, Int. J. of Solids and Structures Vol. 18, No.12,pp. 1145-1152, 1982.
6) Achenbach, J. D., Gautesen, A. K., and McMaken, H. : Diffraction of point-source signals by a circular crack, Bull. Seism. Soc. Amer. 68, pp. 889-905, 1978.
7) Visscher, W. M. : Theory of scattering of elastic waves from flat cracks of arbitrary shape, Wave Motion 5, pp. 15-32, 1983.
8) Boström, A., and Olsson, P. : Scattering of elastic waves by non-planar cracks, Wave Motion 9, pp. 61-76, North-Holland, 1987.
9) Bond, L. J., Punjani, M., and Saffari, N. : Ultrasonic wave propagation and scattering using explicit finite difference methods, In Mathematical modeling in Non-destructive testing, M. Blakemore and G. A. Georgiou eds, Clarendon Press, 1988.
10) Oshima, T., Mikami, S., Nomachi, S. G. : Analysis of Stress Wave Propagetion in Composite Rectangular Beam in the Case of Ultrasonic Pulse Method, Proc. of JSCE, No. 416/I-13, 1990.
11) Hirose, S., and Achenbach, J. D. : Time domain boundary element analysis of elastic wave interaction with a crack, International Journal for Numerical Methods in Engineering, Vol. 28, pp. 629-644, 1989.
12) Kitahara, M., and Nakagawa, K. : BEM application to phase shift analysis, Boundary Elements XII (Eds., Tanaka, M. et al.), Vol. 1, pp. 581-592, Comp. Mech. Publications,Southampton, 1990.
13) Nishimura, N., and Kobayashi, S. : Further applications of regularized integral equations in crack problems, Proc. 2nd IABEM symp., 1990.
14) Ootsuki, A., and Harumi, K. : Effect of Topology and Sub-Surface in Homogenities on Seismic SV Waves, Eng. Struct. Dynam., 11 : 441, 1983.
15) Harumi, K. : Computer Simulation of Ultrasonics in a Solid, NDT Int. 19 (5) ; 315, 1986.
16) Harumi, K., and Uchida, M. : Computer Simulation of Ultrasonics and Its Applications, Journal of Non-destructive Evaluation, Vol. 9, Nos. 213, 1990.
17) Rose J. H. : Elastic wave inverse scattering in nondestructive evaluation, PAGEOPH, Vol. 131, pp. 715-739, 1989.
18) Kunar, R. R., and Rodriguez-Ovejero, L. : A model with non-reflecting boundaries for use in explicit soil-structure interaction analysis, Earthquake Eng. and Structural Dynamics, Vol, 8, pp. 361-374, 1980.
19) Japan Society for Non-destructive Inspection 210 202 Sub Committee WG : Hand Book for Tip Echo Method, Apr, 1987 (in japanese).

(Received December 10, 1991)

超音波パルスエコー法の数値シミュレーション

三木　千寿・池田　清宏・舘石　和雄・高橋　政則

本論文では，鋼構造物のクラックや欠陥の定量的非破壊評価法の開発を目指して超音波パルスエコー法の数値シミュレーション実験を行った．様々な欠陥を有した方形領域に対して，振動方程式を有限要素法を用いて解いた．垂直法，斜角法での入射は境界面を時間差をつけて加振し，シミュレートした．波動の，欠陥による伝播，反射，散乱の性状を調べ，クラックの深さを算出できた．また，実験値との比較によって本解析の妥当性を示した．